

Tissue Tapes—Phenolic Hyaluronic Acid Hydrogel Patches for Off-the-Shelf Therapy

Jisoo Shin, Soojeong Choi, Jung Hyun Kim, Jung Ho Cho, Yoonhee Jin, Suran Kim, Sungjin Min, Su Kyeom Kim, Donghoon Choi,* and Seung-Woo Cho*

Hydrogels have been applied to improve stem cell therapy and drug delivery, but current hydrogel-based delivery methods are inefficient in clinical settings due to difficulty in handling and treatment processes, and low off-the-shelf availability. To overcome these limitations, an adhesive hyaluronic acid (HA) hydrogel patch is developed that acts as a ready-to-use tissue tape for therapeutic application. The HA hydrogel patches functionalized with phenolic moieties (e.g., catechol, pyrogallol) exhibit stronger tissue adhesiveness, greater elastic modulus, and increased off-the-shelf availability, compared with their bulk solution gel form. With this strategy, stem cells are efficiently engrafted onto beating ischemic hearts without injection, resulting in enhanced angiogenesis in ischemic regions and improving cardiac functions. HA hydrogel patches facilitate the *in vivo* engraftment of stem cell-derived organoids. The off-the-shelf availability of the hydrogel patch is also demonstrated as a drug-loaded ready-made tissue tape for topical drug delivery to promote wound healing. Importantly, the applicability of the cross-linker-free HA patch is validated for therapeutic cell and drug delivery. The study suggests that bioinspired phenolic adhesive hydrogel patches can provide an innovative method for simple but highly effective cell and drug delivery, increasing the off-the-shelf availability—a critically important component for translation to clinical settings.

various polymers, they can protect administered cells from harsh conditions (e.g., inflammation, hypoxia) in injured tissues and facilitate cell localization to the target regions.^[1b,2] Hydrogels can also protect labile drugs *in vivo* and enable sustained and controlled drug release to extend their effectiveness.^[3] Despite these benefits, concerns about unfavorable events induced by needle stabbing, such as secondary tissue damage and hemorrhage, remain.^[4] In addition, because the volume of hydrogel that can be injected into dynamic tissues, such as myocardium, is limited due to hydrogel-induced pressure stress on the tissue, the amount of transplantable cells and loaded drugs is also limited. Accordingly, stem cell therapy and drug delivery systems using hydrogels typically cover only a limited area of the defective region.^[5] Because of the complicated processes for hydrogel preparation, handling, and cell/drug loading into hydrogels, most of the current injectable hydrogel systems lack off-the-shelf availability, which hinders their translation to clinical settings.^[4,6] Thus, there have been

few commercialized hydrogel products ready-to-use for clinical cell therapy and drug delivery to address ischemic diseases and wounds.

To overcome these limitations, our group developed a bioinspired, tissue-adhesive hyaluronic acid (HA) hydrogels

1. Introduction


Injectable hydrogels have been actively tested for improving delivery of stem cells and drugs into defective tissues for the treatment of ischemic diseases and wounds.^[1] Prepared from

Dr. J. Shin, S. Choi, J. H. Cho, Dr. Y. Jin, S. Kim, S. Min, S. K. Kim, Prof. S.-W. Cho

Department of Biotechnology
Yonsei University

50 Yonsei-ro, Seodaemun-gu, Seoul 03722, Republic of Korea
E-mail: seungwoocho@yonsei.ac.kr

J. H. Kim, Prof. D. Choi
Division of Cardiology
Department of Internal Medicine
Severance Cardiovascular Hospital
Yonsei University College of Medicine
Seoul 03722, Republic of Korea
E-mail: cdhlyj@yuhs.ac

 The ORCID identification number(s) for the author(s) of this article can be found under <https://doi.org/10.1002/adfm.201903863>.

Prof. S.-W. Cho
Center for Nanomedicine
Institute for Basic Science (IBS)
Seoul 03722, Republic of Korea

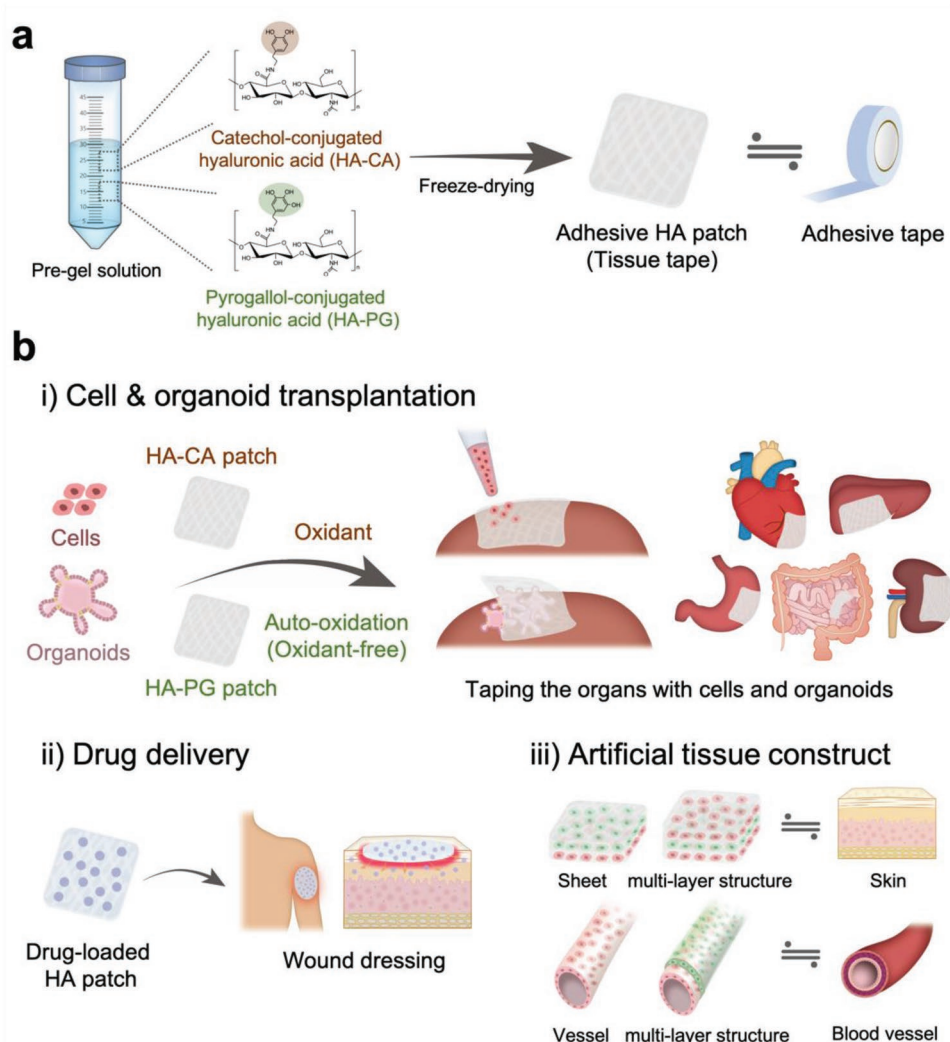
Prof. S.-W. Cho
Yonsei-IBS Institute
Yonsei University
Seoul 03722, Republic of Korea

DOI: 10.1002/adfm.201903863

for injection-free therapy.^[7] The catechol-modified HA (HA-CA) hydrogel was confirmed to be highly biocompatible and tissue adhesive and improved survival and functionality of stem cells compared with conventional photopolymerized HA hydrogels,^[7a,8] which enhanced regenerative efficacy of stem cell therapy in animal models with several types of tissue injuries.^[7a,8b] Likewise, the pyrogallol-modified HA (HA-PG) hydrogel exhibited excellent biocompatibility and tissue adhesiveness enabling noninvasive cell therapy.^[7b] Because of the presence of the catechol or pyrogallol functional group with high binding affinity to various nucleophiles (e.g., amines, thiol, imidazole, etc.), bioinspired HA-CA/PG hydrogels significantly reduce the initial burst of loaded growth factors and improve drug release profiles for sustained delivery.^[7b,8b] Furthermore, because of their excellent tissue adhesiveness, HA-CA/PG hydrogels can mediate safe and efficient delivery of stem cells/growth factors into defective tissue in an injection-free manner by simply depositing the stem cell/growth factor-laden HA hydrogel onto the tissue surface.^[7,8b,9]

Despite the advantages of our HA-CA/PG hydrogels, the injection-free HA hydrogel system still requires technical improvement to advance to the clinical trial stage owing to the technical difficulty in gelation and handling. Clinicians and surgeons—the final users of hydrogels for stem cell therapy and drug treatment—may have difficulty in finding optimal hydrogel loading time owing to its rather tricky oxidation-dependent gelation process. Because the viscosity of HA-CA/PG hydrogels gradually increases after initiating gelation,^[7] it is also critical to determine the optimal viscosity that will facilitate tight adherence to target tissue while not sliding off the tissue before being completely gelled. The HA-CA/PG hydrogels need to be transformed into an off-the-shelf format ready for clinicians.

Herein we developed a novel hydrogel system to facilitate clinically relevant stem cell and drug therapies by changing the format of our HA-CA/PG hydrogels from a solution-based gel to a lyophilized patch (Scheme 1). With the patch, we simply engraft stem cells onto a beating ischemic heart by placing the



Scheme 1. Adhesive HA patch platform for versatile biomedical applications. a) Fabrication of HA-CA and HA-PG patches as a tissue tape. b) Various applications of oxidant-dependent HA-CA patch and oxidant-free HA-PG patch; i) transplantation of single cells and massive cell clusters (organoids) to various types of organ, ii) sustained drug delivery system for wound healing, and iii) construction of multilayered tissue structures such as skin and blood vessel.

adhesive HA patches on the surface of the myocardium wall and then pouring cells on top of the adhered patches. Most importantly, the procedure for stem cell transplantation using this system is much easier and faster than for the HA hydrogel solution, because it does not require cell resuspension in the hydrogel and the critical determination of the optimal loading time and viscosity of HA hydrogel. Interestingly, the HA patch form exhibited greater tissue adhesiveness (HA-CA; approximately fourfold, HA-PG; approximately twofold) and elastic modulus (HA-CA; \approx 40-fold, HA-PG; \approx 12-fold) than the HA gel form, which enabled the stem cell–holding HA patches to adhere tightly and stably onto the dynamic tissue surface without any additional fixation methods. The therapeutic effectiveness of stem cell transplantation using this off-the-shelf adhesive HA hydrogel patch was proven in a rat model of myocardial infarction. We also tested the HA hydrogel patches for cell transplantation to other tissues, including with cell types that are difficult to transplant with conventional injectable hydrogels (e.g., stem cell–derived organoids). In addition to its application for stem cell therapy, the feasibility of the HA hydrogel patch as an effective drug delivery system with off-the-shelf availability was validated in a skin wound healing model. Finally, the platform of cross-linker-free HA hydrogel patch was tested for cell transplantation and drug delivery to completely remove potential safety issues originating from the use of cross-linking agents.

2. Results and Discussion

2.1. HA-CA Patch Preparation for Stem Cell Therapy

Stem cell transplantation and drug delivery are much easier, faster, and safer using HA-CA patches than conventional

methods. Tissue adhesive HA-CA patches were prepared by freezing and lyophilizing the HA-CA solution on a plate (Figure 1a and Figure S1a, Supporting Information). The patch could then be cut into desired shapes and sizes before use (Figure S1b, Supporting Information). HA-CA patches strongly bound to the tissue surface owing to their high tissue adhesiveness. Then, cell-containing medium was added to the patch (Figure S1c and Movie S1, Supporting Information). Because of its high water absorption capacity, lyophilized HA-CA efficiently soaked up the cell solution. Lastly, oxidizing agent (sodium periodate; NaIO_4) was sprayed onto the cell-loaded HA-CA patch to induce cross-linking of the HA-CA (Figure S1c and Movie S1, Supporting Information). Thus, the lyophilized HA-CA patch was transformed into a highly adhesive three-dimensional (3D) hydrogel loaded with cells, enabling facile cell delivery without tissue damage or bleeding. Human adipose-derived stem cells (hADSCs) were mostly viable on the HA-CA patches, similar to those encapsulated in HA-CA hydrogel, confirming that the HA-CA hydrogel patch is biocompatible for cell transplantation (Figure S2, Supporting Information). These characteristics—simple, fast and biocompatible—suggest that HA-CA hydrogel patches can be a user-friendly scaffold for clinicians, surgeons, and researchers.

HA-CA patch fabrication is simple and cost-effective. Furthermore, their dimensions are dependent on the mold size and volume of the HA-CA solution; thus, there is no theoretical limit to their size and shape, which would be highly advantageous for scale-up and mass production. Herein, the large HA-CA patch (100 mm diameter) was prepared on a 100 mm plate and applied onto porcine heart ex vivo (Figure S1d, Supporting Information). The left ventricular wall of the porcine heart was fully covered by the HA-CA hydrogel patch (Figure S1d, Supporting Information), which indicates the scale-up

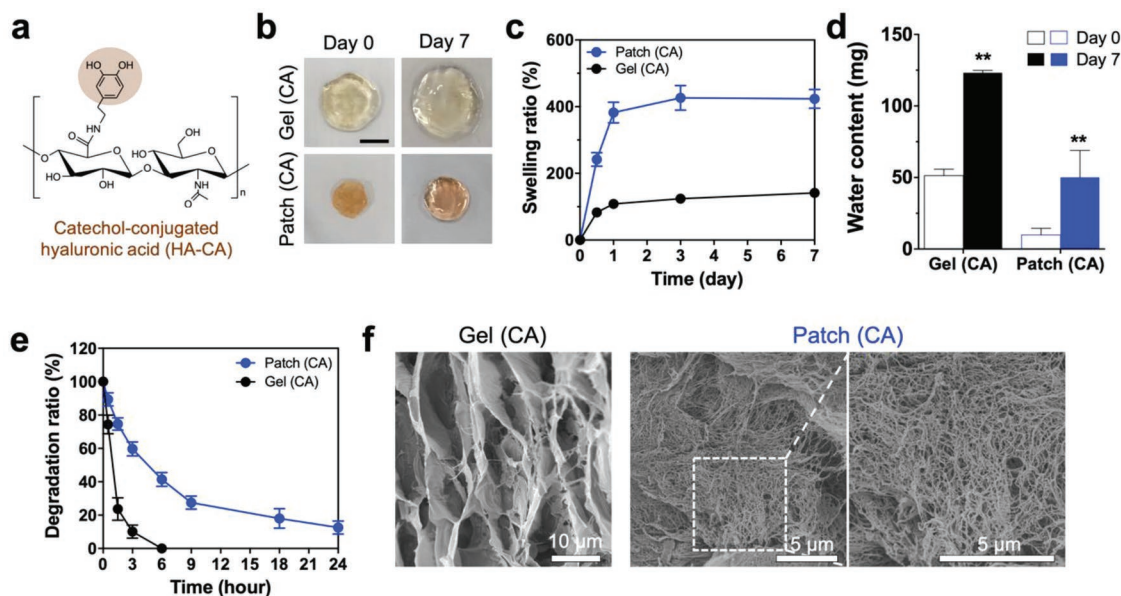


Figure 1. Comparison of the physical and structural characteristics of HA-CA patches and bulk solution hydrogel. a) Chemical structure of HA-CA conjugate. b) Photos of the patch and bulk solution types of HA-CA hydrogels before (day 0) and after (day 7) swelling in PBS at 37 °C. c) The swelling ratios of HA-CA bulk gels and patches upon incubation in PBS at 37 °C ($n = 3$). d) The water contents in HA-CA bulk gels and HA-CA patches at day 0 and 7 in PBS at 37 °C ($n = 3$). e) The degradation profiles of HA-CA bulk gels and HA-CA patches after hyaluronidase (100 U mL^{-1}) treatment ($n = 3$). f) SEM images showing internal structures of HA-CA patches and bulk hydrogels. Scale bars = 10 μm (left panel), 5 μm (middle panel), and 5 μm (right panel).

feasibility of HA-CA patches for clinical settings that require covering large areas of defective tissue with cell- or drug-based therapies. Thus, HA-CA hydrogel patches could provide substantial technical advantages for increasing the effectiveness of stem cell- and drug-based therapies for human applications.

2.2. Comparison of the Physical Properties of the HA-CA Patch and Gel

Changing the HA-CA from a bulk hydrogel solution to a solid patch considerably altered its physical and structural characteristics. The swelling properties of each form were determined by measuring their wet weights during 7 d of incubation under physiological conditions (phosphate buffered saline (PBS) at 37 °C) (Figure 1b). Both HA-CA constructs reached swelling equilibrium after 3 d of incubation (Figure 1c) and remained stable without weight loss or structural deformation up to 7 d (Figure 1b,c). The volume and water content of fully swollen HA-CA patches were less than the fully swollen HA-CA hydrogel (Figure 1b,d). However, the HA-CA patch showed greater swelling capacity (day 7- Patch: $423.5 \pm 48.5\%$; Gel: $141.5 \pm 22.5\%$) (Figure 1c). Because swelling ratio is the ratio of the dried weight on day 0 (W_i) to the swollen weight (W_s), the greater swelling ratio of the HA-CA patch was probably due to having lower water content in its lyophilized state at day 0 compared to the hydrogel (Figure 1d).

The HA-CA patch showed an improved degradation profile compared to the bulk gel. When exposed to enzymatic degradation with hyaluronidase (100 U per sample), the weight loss of the patch was much slower than that of the hydrogel (Figure 1e). The HA-CA hydrogel completely degraded after 6 h while the patch persisted during the 24 h incubation with hyaluronidase (Figure 1e). This result may be due to differences in their internal structures. The scanning electron microscopy (SEM) images indicate that the HA-CA hydrogel is microporous, while the patch possesses nanofibrous structures that are much denser and tighter HA networks (Figure 1f). The additional freezing step during fabrication may also contribute to the structural features of the HA-CA patch. Because oxygen dissolution is usually inversely proportional to solution temperature,^[10] the catechol group of the HA-CA solution might be exposed to mild oxidation during freezing, leading to partial cross-linking between catechol groups and subsequent generation of highly dense nanofibrous structures.

To compare more accurately the porosity and porous structures of HA-CA patch and bulk hydrogel, the diffusion profiles of fluorescein isothiocyanate (FITC)-conjugated dextran (FITC-dextran) across the hydrogels were examined. To this end, diffusion test of FITC-dextran molecules (20 and 70 kDa) was conducted in a Transwell system with membrane insert with HA-CA patch and bulk hydrogels as diffusion barriers (Figure S3a, Supporting Information). We found that FITC-dextran (20 kDa) with a lower molecular weight diffused much faster and in larger quantities through the HA-CA barriers than FITC-dextran (70 kDa) with a higher molecular weight (Figure S3b, Supporting Information). The amount of diffused FITC-dextran molecules (20 and 70 kDa) across the HA-CA patch barriers was significantly less than that of FITC-dextran across the

HA-CA bulk gel barriers (Figure S3b, Supporting Information). This result may suggest again that HA-CA hydrogel in a form of lyophilized patch possesses much denser internal polymer networks comprising nanofibrillar structures compared to HA-CA hydrogel prepared with bulk solution.

Such structural features of HA-CA patch could increase the exposure of functional groups and adhesive moieties on the surface of the patch. The surface compositions of HA-CA patch and bulk hydrogel were analyzed using X-ray photoelectron spectroscopy (XPS). In XPS analysis, the C1s spectrum of HA-CA patch and bulk hydrogel presented five common peaks associated with C=C, C–C, C–OH, C=O, and O–C=O bonds (Figure S4a, Supporting Information). The HA-CA patch showed a relatively higher content of C–OH and C=O bonds and a lower content of C–C bond, compared with the bulk HA-CA hydrogel, indicating that catechol groups and their oxidized quinone state were more abundant on the surface of HA-CA patch than on that of bulk hydrogel. Moreover, the O1s spectrum presenting two typical peaks corresponding to C–OH and C=O denoted that the fraction of C=O bond, representing quinone formation, and the fraction of C–OH bond, representing catechol moiety, were relatively larger and smaller in HA-CA patch, respectively, compared with HA-CA bulk hydrogel (Figure S4b, Supporting Information). Taken together, these observations indicate that functional groups and chemical moieties (e.g., oxidized catechols, quinone) for cross-linking and interaction with nucleophiles exist more abundantly on the surface of HA-CA patch than on that of HA-CA bulk gel, probably due to much larger surface area resulting from highly dense nanofibrillar internal structures in the patch. Increased surface exposure of functional groups and adhesive moieties by lyophilization process to prepare HA-CA patch can induce more robust cross-linking and promote interaction with proteins/peptides, thereby improving mechanical properties and tissue adhesiveness of the patch.

2.3. Improved Tissue Adhesiveness and Elastic Modulus of HA-CA Hydrogel Patch

The HA-CA patches exhibited improved tissue adhesiveness compared to the bulk gel. As we demonstrated previously, the HA-CA hydrogel is highly adherent via oxidized catechol-mediated binding to nucleophiles (e.g., amines, thiol, and imidazole) in peptides/proteins on tissue surfaces.^[11] To compare the tissue adhesion strengths of the HA-CA patch and bulk gel, we measured the force required to detach the HA-CA adhesives from porcine heart tissues using a tack test method (Figure 2a). The tissue-adhesive strength of the patch (5.5 ± 0.2 N) was more than threefold greater than that of the gel (1.5 ± 0.7 N) (Figure 2b,c). Once the lyophilized HA-CA patch contacted wet tissue, it soaked up water on the tissue surface, which facilitated a tight wet adhesion between the HA-CA patch and the tissue surface.^[12] Compared to the microporous structure of the hydrogel, the highly dense nanofibrous polymer networks of the patch may increase the adhesive surface area (Figure 1f), which would also improve adhesiveness. The adhesive strength of the patch overwhelmed the acrylic glue used to fix the tissue to the probe, as evidenced by tissue detachment

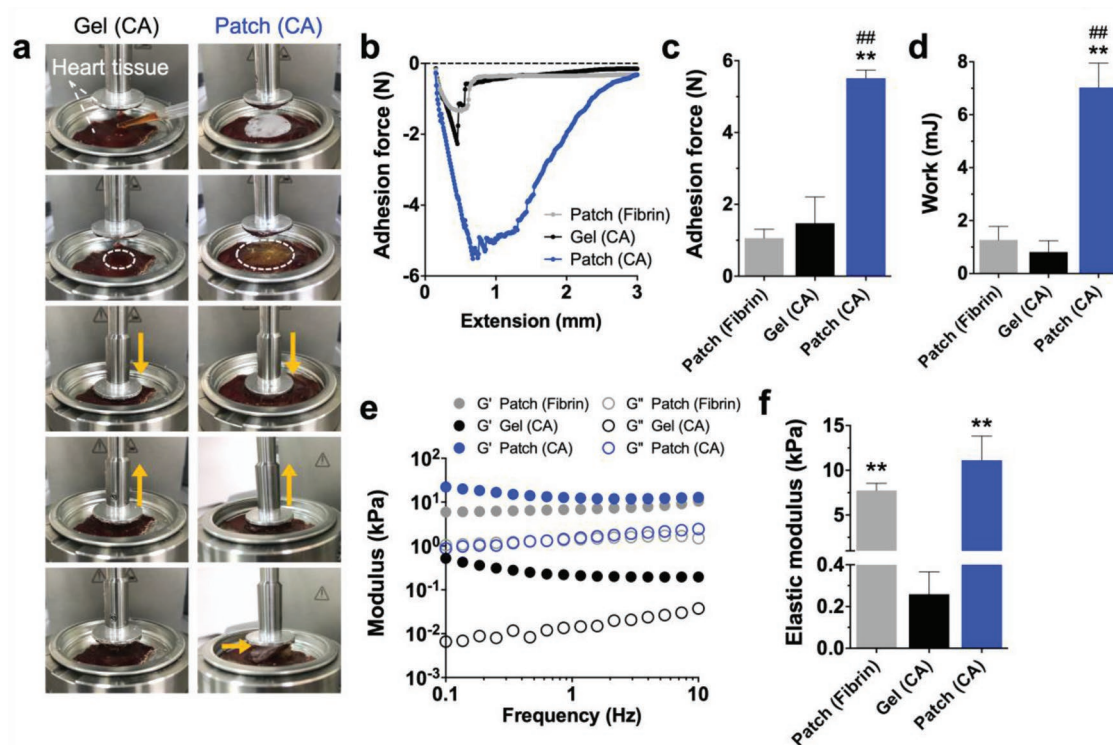


Figure 2. Comparison of tissue adhesion and mechanical properties of HA-CA patches, bulk hydrogels, and commercial fibrin sealant patches. a) Photos showing tack test processes for measuring adhesion strength of HA-CA bulk solution- and patch-type hydrogels to porcine heart tissue. b) The adhesion strength curves of HA-CA patches, bulk gels, and fibrin patches to porcine heart tissue measured by a rheometer in tack test mode. c) Average adhesion strengths of HA-CA patches, bulk gels, and fibrin patches to porcine heart tissue ($n = 3$, $**p < 0.01$ vs Gel, $##p < 0.01$ vs Fibrin patch). d) The average work for the adhesion of HA-CA patches, bulk gels, and fibrin patches on porcine heart tissue ($n = 3$, $**p < 0.01$ vs Gel, $##p < 0.01$ vs Fibrin patch). e) Rheological analysis of the elastic moduli of HA-CA patches, bulk gels, and fibrin patches performed in frequency sweep mode. f) The average elastic moduli of HA-CA patches, bulk gels, and fibrin patches at 1 Hz ($n = 3$, $**p < 0.01$ vs Gel).

from the probe prior to cohesive and adhesive failure of the patch (Figure 2a). The energy necessary to detach the adhesive HA-CA patch from heart tissue was determined by calculating the area under the force-extension length curve (Figure 2b). Much more energy (approximately sevenfold) was needed to detach the patch (7.1 ± 1.3 mJ) from heart tissue than the bulk hydrogel (0.9 ± 0.6 mJ) (Figure 2d), indicating stronger adhesion between the patch and tissue. When we compared the adhesiveness of two types of HA-CA hydrogels (patch and bulk gel) to stainless metal substrate, the results showed a similar tendency to those from tissue-adhesion test (Figure S5, Supporting Information). The HA-CA patch hydrogel also showed significant improvement in mechanical properties compared with the bulk hydrogel. Similar to the bulk hydrogel, the patch hydrogel possessed stable internal networks of cross-linked HA polymers. The patch had a greater storage modulus (G') than loss modulus (G'') at all tested frequency (Figure 2e). The average elastic modulus of the patch (11.12 ± 2.71 kPa) was much greater (≈ 40 -fold) than that of the bulk hydrogel (0.26 ± 0.11 kPa) (Figure 2f).

Interestingly, tissue adhesive property of HA-CA patches was even better than that of commercial patch products. Mechanical properties and adhesion strength of our HA-CA patch system were compared with those of commercial fibrin sealant patch for clinical use. HA-CA patch (11.12 ± 2.71 kPa)

was found to have higher elastic modulus than fibrin patch (7.75 ± 0.80 kPa), but there was no significant difference ($p > 0.05$) between two patch groups (Figure 2e,f). In terms of tissue adhesiveness, however, HA-CA patch was superior to the fibrin patch (Figure 2b–d). The tissue-adhesion force of fibrin patch (1.1 ± 0.2 N) was similar to that of HA-CA bulk hydrogel (1.5 ± 0.7 N), which was much weaker than that of HA-CA patch (5.5 ± 0.2 N) (Figure 2c). These results support our claim that the developed HA-CA patch system can provide advanced therapeutic platform for clinical application. Given the marked improvement in tissue adhesiveness and elastic modulus of the HA-CA patch over the bulk gel and commercially available patch, we anticipate our patch will be better retained on dynamically beating heart tissue without hydrogel deformation and graft failure, and would accordingly be a more suitable scaffold for cell therapy with enhanced and prolonged regenerative efficacy.

2.4. Stem Cell Therapy Using HA-CA Hydrogel Patch for Myocardial Infarction

Next, we tested the feasibility of the HA-CA patch for stem cell therapy in ischemic diseases. Rat bone marrow-derived mesenchymal stem cells (BM-MSCs), which can induce therapeutic

angiogenesis and tissue regeneration via paracrine secretion of multiple angiogenic factors,^[13] were transplanted into the ischemic myocardium of a rat myocardial infarction model using the HA-CA patch or by direct intramyocardial injection. Myocardial infarction in a rat heart was induced by ligating left anterior descending coronary artery (LAD), followed by reperfusion.^[14] Animal experiments included four groups: i) saline, ii) HA-CA patch only (patch only), iii) direct intramyocardial injection of BM-MSCs (MSC-injection), and iv) BM-MSC-loaded HA-CA patch (MSC-patch). Equal numbers of cells (2.0×10^5) were administered in the experimental groups during BM-MSC transplantation.

The HA-CA patch mediated successful engraftment of BM-MSCs onto the ischemic hearts as shown in Movie S1 (Supporting Information). Hematoxylin and eosin (H&E) staining of the retrieved hearts 3 d after transplantation showed that the MSC-laden HA-CA patches tightly adhered onto the surface of the ischemic hearts (Figure 3a). Thus, the adhesion strength of the patch was strong enough to support wet adhesion to a dynamically beating heart. To track the transplanted stem cells, BM-MSCs were labeled with the fluorescent cell tracer, Paul

Karl Horan 26 (PKH26), before transplantation. PKH26-labeled BM-MSCs were detected in the ischemic myocardium by 2 weeks after cell transplantation using the patch, indicating efficient migration of the BM-MSCs from the patch on the outer heart wall into the ischemic region (Figure 3b). A larger number of PKH26-labeled cells were observed in the MSC-patch group than the MSC-injection group (Figure 3c), confirming that the hydrogel patch is a functional scaffold for supporting cell survival and improving engraftment of transplanted cells.

To investigate the therapeutic effects of HA-CA patch-mediated transplantation of BM-MSCs on improving cardiac function of ischemic heart, echocardiography was performed 4 weeks after transplantation. After myocardial infarction by LAD occlusion, left ventricle (LV) hypertrophy and deterioration of cardiac function are usually observed.^[15] Four weeks after BM-MSC transplantation using the patch, the LV internal dimension during systole (LVIDs) was notably decreased (4.1 ± 0.5 mm) compared to other control groups (saline injection; 6.1 ± 1.8 mm, patch only; 6.0 ± 1.4 mm, and MSC-injection; 5.4 ± 1.4 mm) (Figure 3d). The LV internal

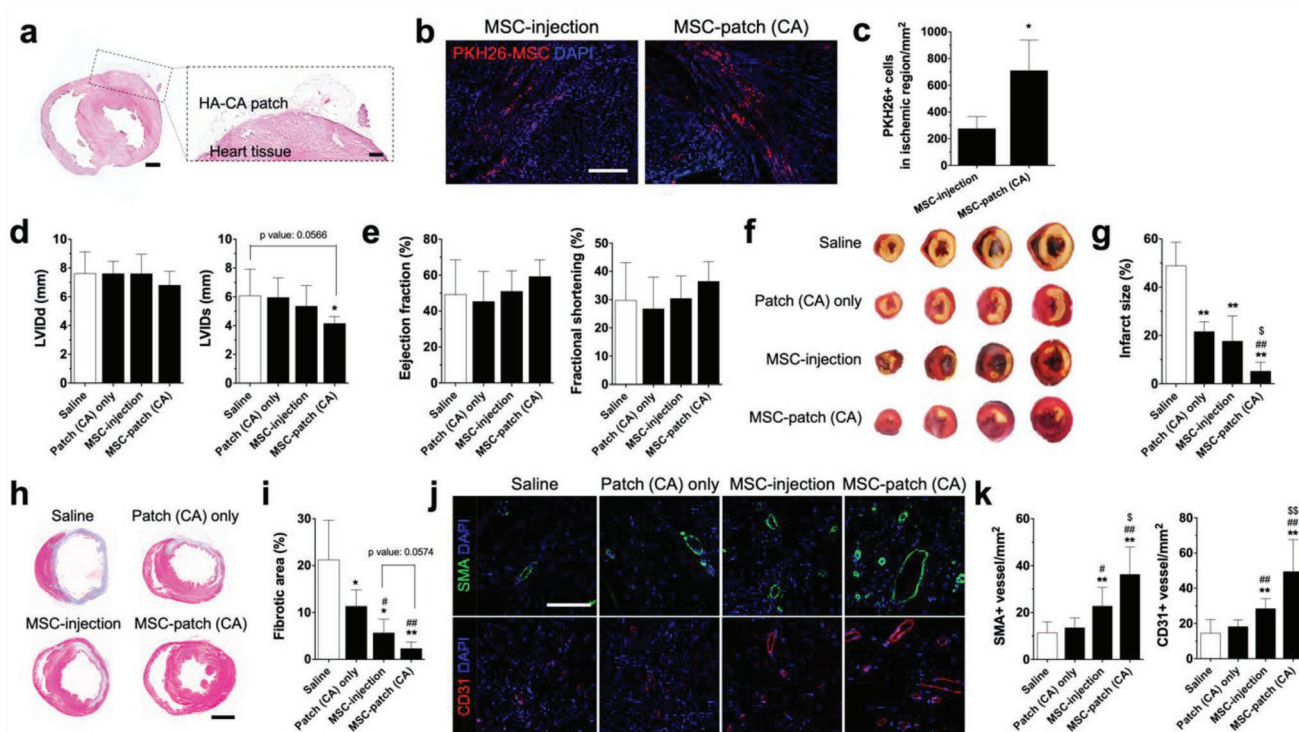


Figure 3. Stem cell therapy using tissue adhesive HA-CA hydrogel patches in a rat myocardial infarction model. a) H&E staining of BM-MSC-laden HA-CA patches adhered onto the ischemic heart wall 3 d after transplantation. Scale bars = 5 mm (left) and 1 mm (right). b) Immunofluorescence images of PKH26-labeled BM-MSCs in the infarcted region of the myocardium of MSC-injection and MSC-patch groups 2 weeks post-transplantation. Scale bar = 200 μ m. c) Quantification of PKH26-positive cells in infarcted myocardium 2 weeks after treatment ($n = 3$, $*p < 0.05$ vs MSC-injection). Echocardiographic analysis to evaluate LV functions 4 weeks post-treatment; d) LV inner diameter at end diastole (LVIDd) (left) and LV inner diameter at end systole (LVIDs) (right) ($n = 4-6$, $*p < 0.05$ vs Patch only), e) ejection fraction (EF) (left) and fractional shortening (FS) (right) ($n = 5-6$). f) TTC staining images of heart slices retrieved 4 weeks after treatments to detect infarcted area (yellow–white colored region). g) Average infarcted size quantified from the TTC-stained heart slice images ($n = 5$, $**p < 0.01$ vs Saline, $##p < 0.01$ vs Patch only, and $\$p < 0.05$ vs MSC-injection). h) Masson's trichrome staining images of sectioned heart tissues 4 weeks post-treatment. Scale bar = 1 cm. i) Quantification of fibrotic area in infarcted myocardium based on Masson's trichrome-stained images ($n = 5$, $*p < 0.05$ and $**p < 0.01$ vs Saline, $\#p < 0.05$ and $##p < 0.01$ vs Patch only). j) Images showing immunofluorescence staining for α -SMA (arterioles; upper) and CD31 (capillaries; bottom) in ischemic region 4 weeks after treatments. Scale bar = 100 μ m. k) Quantification of α -SMA-positive arterioles (left) and CD31-positive capillaries (right) in infarcted myocardium ($n = 7-15$, $**p < 0.01$ vs Saline, $\#p < 0.05$ and $##p < 0.01$ vs Patch only, and $\$p < 0.05$ and $$$p < 0.01$ vs MSC-injection).

dimension at diastole (LVIDd) was also decreased by BM-MS-C transplantation with the patch (Figure 3d). Ejection fraction (EF) and fractional shortening (FS) of the ischemic hearts were also improved (Figure 3e). These results demonstrate that the noninvasive HA-CA patch-mediated stem cell therapy could prevent LV dilatation and cardiac hypertrophy following myocardial infarction and restore cardiac function.

Stem cell therapy with adhesive HA-CA hydrogel patch significantly reduced fibrosis and infarct size in ischemic myocardium. The infarcted region in the LV was visualized and quantified by triphenyltetrazolium chloride (TTC) staining. Infarct size was significantly smaller in the MSC-patch group than the control groups ($6.1 \pm 3.4\%$ vs $50.3 \pm 10.7\%$ (saline), $21.6 \pm 4.1\%$ (patch only), and $17.6 \pm 9.4\%$ (MSC-injection)) (Figure 3f,g), indicating that infarct spreading could be attenuated by HA-CA patch-mediated MSC transplantation. Masson's trichrome (MT) staining of infarcted hearts revealed that fibrotic scar tissue formation in the ischemic myocardium was significantly reduced in the MSC-patch group ($2.3 \pm 1.4\%$), while other control groups exhibited relatively larger fibrotic areas (saline injection, $21.2 \pm 8.4\%$; patch only, $11.3 \pm 3.5\%$; and MSC-injection, $5.7 \pm 2.9\%$) (Figure 3h,i). This significant improvement in therapeutic efficacy of BM-MS-Cs was attributed to the enhanced angiogenesis facilitated by use of the HA-CA patch. MS-Cs promote angiogenesis by secreting many angiogenic growth factors.^[16] Thus, angiogenesis in the infarct region after treatments was assessed by immunohistochemical staining of the arteriole and capillary markers, α -smooth muscle actin (α -SMA) and CD31, respectively (Figure 3j). Numbers of α -SMA- and CD31-positive blood vessels were markedly increased in the MSC-patch group compared to the other groups (Figure 3k), suggesting that use of the patch may have increased paracrine secretion of angiogenic factors by BM-MS-Cs.

Our HA-CA hydrogel patch platform possesses several technical advantages over conventional methods for stem cell transplantation into ischemic hearts. Stem cell therapy using cardiac patches prepared from biocompatible polymers is an important strategy.^[17] Polymeric patch-mediated methods deliver larger numbers of cells and cover much larger areas of ischemic regions compared to injection-based methods. Although stem cell therapy using patch scaffolds has shown promising outcomes in preclinical studies, technical limitations still remain. Most patch scaffolds made of synthetic polymers (e.g., poly(ϵ -caprolactone), polyurethane, and polyethylene glycol) require additional procedures that are technically challenging to stably fix the patches onto the myocardium surface.^[9,18] Attachment of the patches using sutures or glues onto dynamically beating hearts often did not result in tight integration of the patch onto damaged myocardium due to a lack of tissue adhesiveness.^[19] Moreover, sutures may cause tissue damage and hemorrhage, and glues may hinder cell migration from the patch to defected tissue.^[20] Natural polymer-based cardiac patches (e.g., collagen, gelatin, and fibrin) usually have poor mechanical properties and fast degradation rate, which can inhibit long-term therapeutic effects.^[21] Cell sheet transplantation is another important stem cell-based technique for treating myocardial infarction. This scaffold-free cell therapy has been widely applied to deliver diverse types of stem cells onto infarcted heart.^[22] However,

cell death often occurs immediately after transplantation into ischemic myocardium with intensive inflammation and tissue necrosis, leading to graft failure.^[21] More critically, cell sheets do not possess high enough mechanical stability to withstand the contractile forces of a beating heart.^[23] In contrast, our HA-CA hydrogel patch exhibited high elasticity and tissue adhesiveness enough to withstand the pressure and dynamic force exerted by a beating heart, leading to its stable adhesion and integration onto ischemic myocardium and successful cell delivery and engraftment (Figure 3a–c). Therefore, the HA-CA patch provides a novel strategy to replace conventional transplantation methods.

2.5. Organoid Transplantation Using HA-CA Patch to Various Organs

Due to their excellent tissue adhesiveness, HA-CA hydrogel patches can also be applied to other organs or tissues using the same process as was used to apply them to hearts (patch attachment, cell seeding, and oxidizing agent spraying). HA-CA patches loaded with DiI-labeled hADSCs were easily deposited and firmly fixed onto the surface of various other organs, including the liver, intestine, and kidney (Figure 4a). Large cell clusters, such as organoids and spheroids, were also transplanted onto organs using HA-CA patches without injection, infusion, or any invasive procedures. Conventional injection-based methods may be inappropriate for ensuring efficient engraftment of large cell clusters onto target organs due to difficulty in retaining intact structures and viability of cell clusters during injection and possible occlusion by cell clusters after infusion into vessels.^[24] In particular, organoid technology represents a powerful resource for regenerative medicine, but efficient grafting is challenging due to the lack of proper methods and materials for transplantation.^[25] Many studies have tried to transplant organoids using various methods. For instance, intestinal and colon organoids were instilled into colonic lumen as a cell suspension with diluted Matrigel in PBS solution^[26] or directly administered by colonoscopy-guided intramucosal injection.^[27] Although these strategies do not require extensive surgical intervention, engraftment rates were substantially low.^[26,27] Liver organoids were resuspended in cold Matrigel solution and transplanted via injection into the kidney subcapsular space^[28] or intrasplenically for orthotopic transplantation.^[29] All of these methods were unable to deliver the organoids directly to the target tissue or organ, leading to low engraftment and limited regenerative effect.^[29b] In addition, xenogenic matrices derived from animal sources, such as Matrigel, cannot be applied to clinical settings, because of safety issues pertaining to animal pathogen transmission and immunogenicity.^[30]

Thus, we tested HA-CA patch-mediated transplantation of organoids generated from stem cells or reprogrammed cells. Liver organoids derived from reprogrammed hepatocyte-like cells were transplanted using the patch onto the liver of an athymic mouse. Because organoids may not migrate efficiently into liver tissue due to their large size, liver organoids were first placed onto the liver surface, the HA-CA patch was deposited on top, and then oxidizing agent was sprayed on the cell-patch

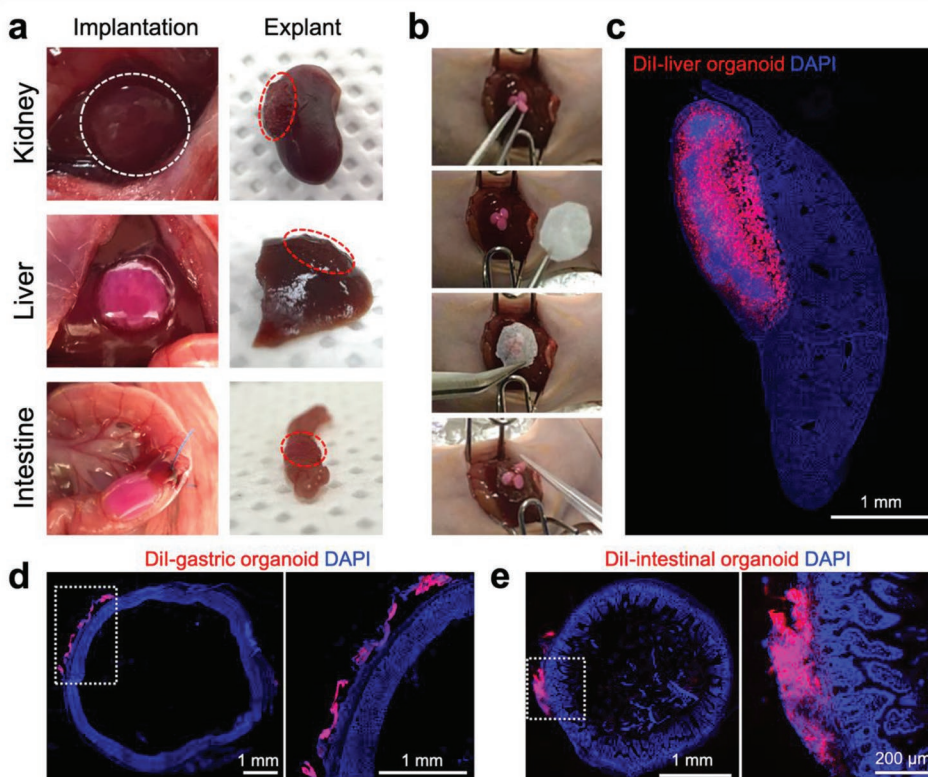


Figure 4. Stem cell and organoid transplantation using HA-CA patches to various organs. a) Gross view images of HA-CA patches containing DiI-labeled hADSCs stably fixed on the tissue surface of various organs in mouse (kidney, liver, and intestine) right after transplantation (left) and the day after transplantation (right). b) Procedures for HA-CA patch-mediated transplantation of liver organoids into the liver of mouse. Fluorescence images to confirm the engraftment of c) DiI-labeled liver organoids onto the mouse liver lobe 7 d after transplantation. Scale bar = 1 mm, d) DiI-labeled gastric organoids onto the surface of mouse stomach 3 d after transplantation. Scale bars = 1 mm, and e) DiI-labeled intestinal organoids onto the surface of mouse intestine 3 d after transplantation. Scale bars = 1 mm (left) and 200 μ m (right).

implants (Figure 4b). Seven days after transplantation, a large mass of DiI-labeled liver organoids was clearly visualized on the liver lobe, indicating successful engraftment of massive organoids into the liver without invasive procedures (Figure 4c). Similarly, gastric and intestinal organoids derived from primary gastric and intestinal stem cells (Figure S6, Supporting Information) were successfully transplanted to target organs of an athymic mouse using the patch. DiI-labeled gastric and intestinal organoids were efficiently engrafted onto the surface of the stomach and small intestine, respectively (Figure 4d,e). As a result, we confirmed that HA-CA hydrogel patch is quite biocompatible and facilitates efficient engraftment of transplanted organoids into different organs, such as liver, intestine, and stomach, without any loss or deformation of organoids in a simple and noninvasive manner (Figure 4c–e). Together, these results suggest that the HA-CA hydrogel patch is a versatile platform for cell therapy regardless of target organ or cell type.

2.6. Topical Growth Factor Therapy Using HA-CA Hydrogel Patches for Wound Healing

HA-CA hydrogel patch could also be applicable for drug delivery system with off-the-shelf availability for clinical setting. Thus,

HA-CA patch was tested for local delivery of vascular endothelial growth factor (VEGF), one of the most potent growth factors for angiogenesis and wound healing process^[31] to determine its applicability for drug delivery. Catechol-based hydrogel systems rarely release encapsulated protein drugs *in vitro* (in the absence of enzymatic treatment for biodegradation) due to strong covalent interactions between the catechol and various nucleophiles within the proteins.^[8b,32] In contrast to the HA-CA bulk gel, which exhibits a low drug release profile, the patch may facilitate the release of protein drugs *in vivo*, because the nanofibrous structures of the patch provide a much larger surface area for drug release to external environments (Figure 1f). The enzyme-linked immunosorbent assay (ELISA) analysis indicated that VEGF in the HA-CA patch was hardly released from the patch during incubation at physiological conditions (in PBS at 37 °C) without hyaluronidase treatment (Figure 5a). In the presence of hyaluronidase (5 U per sample), VEGF was sustainably released from the patch for 9 d due to degradation of the HA hydrogel network (Figure 5a). This result suggests that the sustained and controlled release of the encapsulated growth factor within the patch can be triggered by hyaluronidase activity *in vivo*. Further, to test the HA-CA patch system for ready-to-use, long-lasting VEGF therapy, HA-CA solution containing VEGF was frozen and then lyophilized into the patch

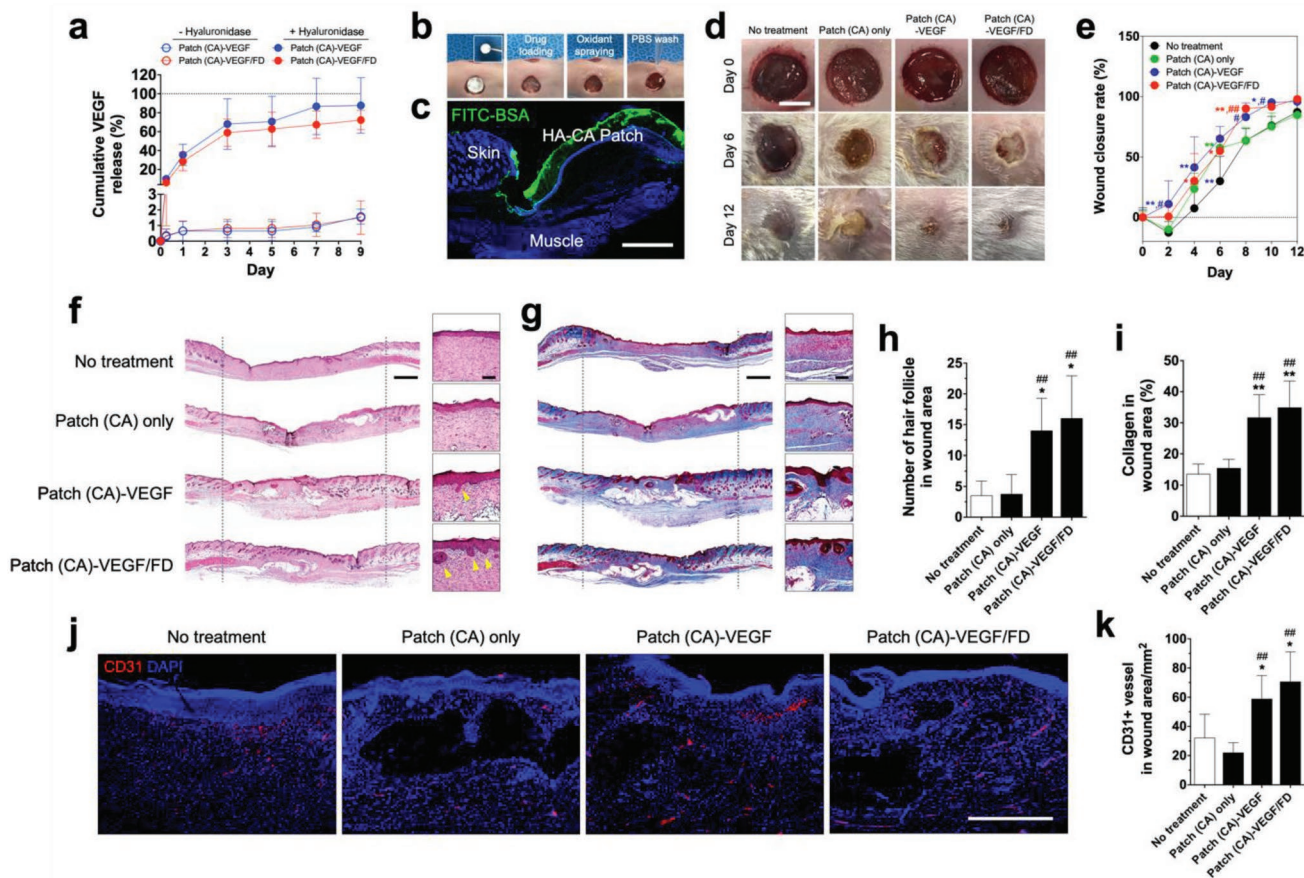


Figure 5. Topical VEGF delivery using HA-CA patches in a skin wound mouse model. a) Release profiles of VEGF from HA-CA hydrogel patches with or without hyaluronidase treatment ($n = 3$). b) Procedures for drug delivery using HA-CA patches on skin wounds. c) Fluorescence image showing tight adhesion of the HA-CA patch carrying FITC-BSA to the wound region. Scale bar = 1 mm. d) Representative gross images of wound closure at day 0, 6, and 12. Scale bar = 5 mm. e) The wound closure rate measured up to day 12 after treatment ($n = 5-6$, $*p < 0.05$ and $**p < 0.01$ vs No treatment, $\#p < 0.05$ and $\#\#p < 0.01$ vs Patch only at each time point). f) H&E-stained images of the treated wounds at day 12. Yellow arrowheads in the right columns indicate regeneration of hair follicles. Scale bars = 1 mm (left column) and 100 μm (right column). g) Masson's trichrome staining images of the treated wounds at 12 d. Collagen is stained blue. Scale bars = 1 mm (left column) and 100 μm (right column). h) Quantification of regenerated hair follicles in wound regions based on H&E-stained images ($n = 3-4$, $*p < 0.05$ vs No treatment and $\#p < 0.05$ vs Patch only). i) Quantification of collagen deposition in wound regions based on Masson's trichrome-stained images ($n = 10-12$, $**p < 0.01$ vs No treatment and $\#\#p < 0.01$ vs Patch only). j) Images showing immunofluorescence staining for CD31 in wound region 12 d after treatments. Scale bar = 500 μm . k) Quantification of CD31-positive vessels in wound site ($n = 4-5$, $*p < 0.05$ vs No treatment and $\#\#p < 0.01$ vs Patch only).

(Patch-VEGF/FD group). These patches preloaded with VEGF showed a similar release profile of VEGF to the HA-CA patch loaded with VEGF after lyophilization (Patch-VEGF group) (Figure 5a), indicating that lyophilization did not affect release of growth factors from the patch.

Using the same process, we also applied HA-CA patches loaded with fluorescently labeled proteins in a mouse model of full-thickness skin wound. The HA-CA patch was placed on the wounded region, FITC-conjugated bovine serum albumin (BSA) (FITC-BSA) was loaded, and then oxidizing agent (NaIO_4) was sprayed to induce gelation (Figure 5b). Fluorescence microscopy images of skin tissues at day 3 confirmed that the FITC-BSA-loaded HA-CA patch adhered tightly to the wounded tissue region and that the FITC-BSA began to diffuse into the wound (Figure 5c). Because of the tight and direct contact between the HA-CA patch and wounded tissue, the loaded drugs were efficiently delivered to the wound, which accelerated healing.

The therapeutic efficacy of the VEGF-loaded HA-CA patch was evaluated in a full-thickness skin wound mouse model. HA-CA patch groups for VEGF delivery included: 1) HA-CA patch preloaded with VEGF before lyophilization (Patch-VEGF/FD group) and 2) HA-CA patch loaded with VEGF after attaching the patch onto the cutaneous wound of mice (Patch-VEGF group). As mentioned above, VEGF encapsulated within HA-CA patch was not released efficiently in *in vitro* conditions due to covalent binding of the catechol group of HA-CA to the protein. However, in wounded skin tissue, which has increased hyaluronidase activity,^[33] encapsulated VEGF might be effectively released via enzymatic degradation as simulated in Figure 5a. Thus, treatments with the HA-CA patch carrying VEGF (Patch-VEGF group and Patch-VEGF/FD group) induced significantly faster wound closure compared to the no treatment or empty HA-CA patch (Patch only) groups (Figure 5d,e). Histological analysis of the wounded tissues retrieved at day

12 after treatment indicated more functional and later stage wound healing in the groups treated with the VEGF-loaded HA-CA patches (Patch-VEGF group and Patch-VEGF/FD group). H&E staining also indicated skin regeneration with larger numbers of newly formed hair follicles in the wound region (Figure 5f,h). MT staining confirmed more extensive collagen deposition in the VEGF-HA-CA patch groups compared to the no treatment and patch only groups (Figure 5g,i). In addition, compared to the no treatment and HA-CA patch only groups, in the VEGF-HA-CA patch groups (Patch-VEGF group and Patch-VEGF/FD group), microvessel formation significantly increased in the wound region as demonstrated by immunohistochemical staining for the capillary marker, CD31, and quantification of CD31⁺ vessels (Figure 5j,k). Importantly, there was no difference in wound healing efficacy between the Patch-VEGF and Patch-VEGF/FD groups. In terms of convenience and off-the-shelf availability for their therapeutic application in human patients, the Patch-VEGF/FD formulation shows greater clinical utility than the Patch-VEGF, because it can be directly applied like a wound dressing without requiring a drug loading step. In addition, the Patch-VEGF/FD formulation showed enhanced therapeutic efficacy in comparison to the conventional drug delivery approach using solution-based HA-CA bulk hydrogel. In a mouse model of full-thickness skin wound, VEGF delivery using HA-CA hydrogel patch accelerated wound closure and induced better healing process, compared to VEGF delivery using HA-CA bulk hydrogel applied through pipetting (Figure S7, Supporting Information). This probably resulted from improved drug delivery efficiency owing to improved tissue adhesion ability and sustained drug release caused by slower degradation of HA-CA patch.

2.7. Transformation of HA-CA Patches for Multicellular Constructs

In addition to their feasibility for noninvasive cell therapy and drug delivery, HA-CA patches can provide technical advantages in preparing multicellular constructs for tissue engineering applications. The multilayered architecture of several tissues (e.g., skin, blood vessel, etc.) can be recapitulated via layer-by-layer stacking of HA-CA patches due to their high adhesive strength. The generation of three- or five-layered HA constructs was shown by loading two different color inks (red and green) on each patch layer (Figure S8a, Supporting Information). Fluorescently labeled hADSCs with two different dyes (DiI; red and CFDA; green) were alternatively seeded onto each layer of HA-CA patch, demonstrating 3D multicellular layer structure (Figure S8b, Supporting Information). HA-CA patches can also be transformed into multilayered tubular (3D vessel-like) structures by wrapping each patch layer onto mandrels (Figure S8c, Supporting Information). The diameter of these blood vessel-like structures is dictated by the size of mandrels. Thus, there is no limit to their dimensions. Using two different color inks (red and green), we confirmed that two-layered vessel-like structures were easily generated without any additional equipment (Figure S8c, Supporting Information). Multilayered tubular structures were mechanically stable and also highly elastic, similar to

blood vessels (Figure S8d, Supporting Information) due to the improved elastic modulus of the HA-CA patch (Figure 2e,f). To reconstitute blood vessel structures with cellular components, human umbilical vein endothelial cells (HUVECs) were loaded onto the inner patch as an intimal layer, and hADSCs were loaded onto the outer patch as a medial layer (Figure S8e, Supporting Information). CFDA-labeled HUVECs were retained along the luminal structures and DiI-labeled hADSCs formed the medial part supporting blood vessel structures (Figure S8e, Supporting Information). Together, these results demonstrate that simple transformations of HA-CA patches can be used to construct tissue-mimicking multilayered structures (e.g., multilayered sheets for skin tissue and multilayered tubes for blood vessel).

2.8. Comparison of Characteristics of the HA-PG Patch and Gel

Through a series of in vitro and in vivo experiments, we showed a great promise for the clinical use of HA-CA patches, but limitations remain to further improve HA-CA patch platform. Oxidative cross-linking of the HA-CA patches requires spraying of an oxidizing agent (sodium periodate; NaIO₄). Previous studies, including ours, have reported that NaIO₄ does not affect cell viability, proliferation, and differentiation in a range of concentrations used to induce oxidative cross-linking for hydrogel formation.^[7a,8,32] In addition, no adverse events, such as tissue damage and inflammation, were observed during whole experimental periods. However, some concerns associated with safety and technical handling may remain due to the use of oxidants in clinical situations. Therefore, modification of the HA with functional moieties capable of generating a hydrogel without oxidants via auto-oxidation in vivo (e.g., pyrogallol (PG) group) could be considered for advanced clinical translation. In our study, to get rid of any safety concerns by oxidants, we tested the PG-modified HA (HA-PG) for oxidant-free hydrogel patch. Since HA-PG has greater oxidation potential than HA-CA does due to additional hydroxyl group of PG group (3 hydroxyl groups in PG vs 2 hydroxyl groups in CA) (Figure 6a and Figure 1a), HA-PG patch would be cross-linked through auto-oxidation by in vivo oxidative environment (e.g., endogenous oxygen species, peroxidase in tissue) even without additional oxidant treatment.

For the experiments under in vitro ambient air condition which does not provide oxidation environment sufficient for auto-oxidation, HA-PG patch and bulk gel were formed by oxidant NaIO₄ (4.5 mg mL⁻¹) treatment (Figure 6b). The patch and bulk gel form of HA-PG showed similar swelling properties under physiological condition (in PBS at 37 °C) (Figure 6c). The HA-PG patch showed much slower enzymatic degradation profile upon hyaluronidase treatment (500 U per sample), compared to the HA-PG bulk gel (Figure 6d). Similar to HA-CA patch, the HA-PG patch also showed significantly improved mechanical properties. Both patch and gel form of HA-PG had a greater storage modulus (G') than loss modulus (G'') at all tested frequency, indicating stable hydrogel formation (Figure 6e). The average elastic modulus of the patch (18.17 ± 4.28 kPa) was much greater (≈12-fold) than that of the bulk hydrogel (1.48 ± 0.09 kPa) (Figure 6f). The improvement

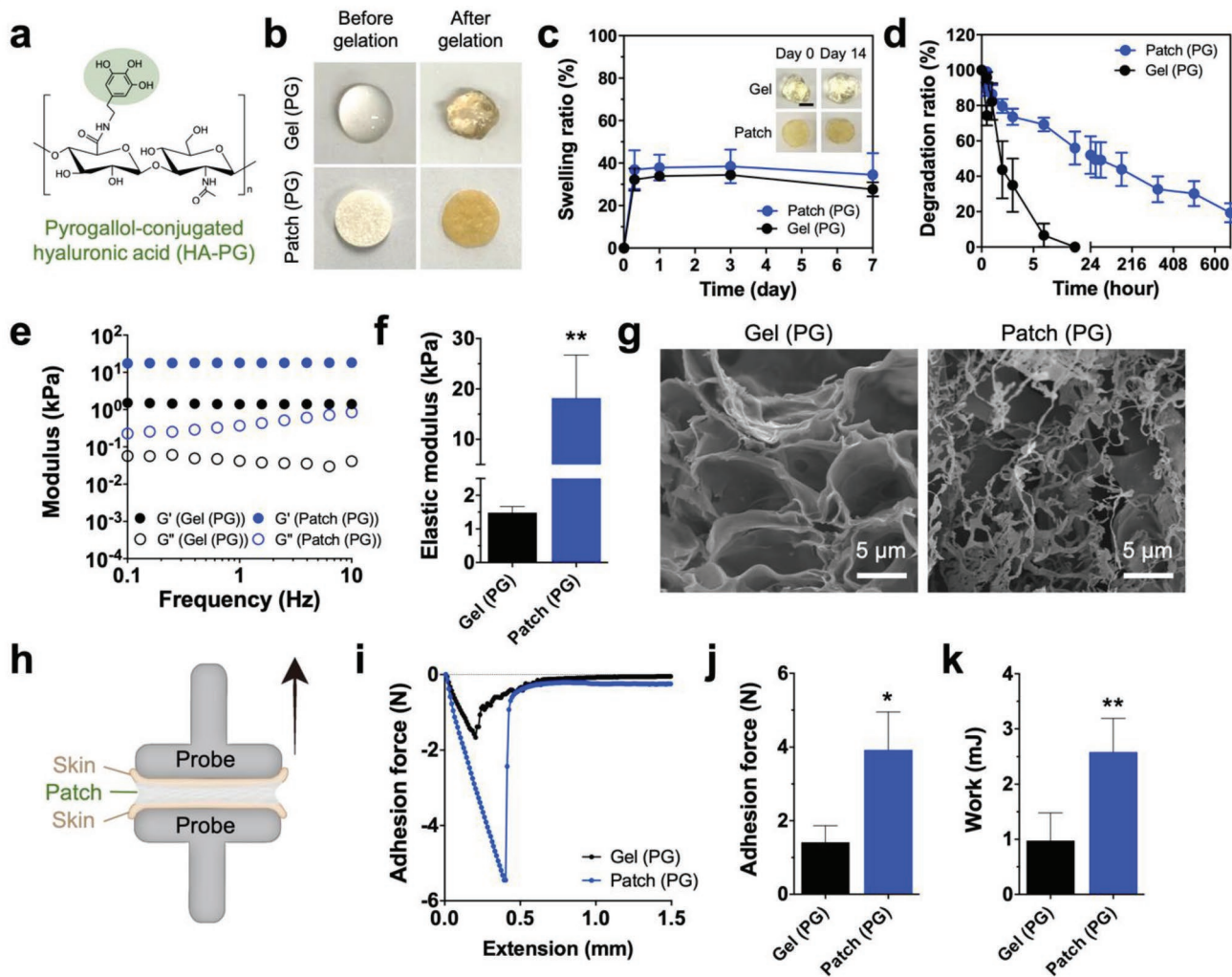


Figure 6. Comparison of the physical, structural, and mechanical characteristics of HA-PG patch and bulk solution hydrogel. a) Chemical structure of HA-PG conjugate. b) Photos of the patch and bulk solution types of HA-PG hydrogels before and after gelation. c) The swelling ratios of HA-PG bulk gels and patches upon incubation in PBS at 37 °C ($n = 4-5$). d) The enzymatic degradation profiles of HA-PG bulk gels and HA-PG patches under 500 U mL⁻¹ of hyaluronidase treatment ($n = 5-6$). e) Rheometric analysis of HA-PG bulk gels and patches in a frequency sweep mode. f) The average elastic moduli of HA-PG bulk gels and patches at 1 Hz ($n = 4$, $**p < 0.01$ vs Gel). g) SEM images for investigating internal structures of HA-PG bulk gels and patches. Scale bars = 5 μ m. h) Schematic illustration of the tissue-adhesion force measurement setup in a tack test mode. i) The adhesion force curves of HA-PG bulk gels and patches to mouse skin. j) Average adhesion strengths of HA-PG bulk gels and patches to mouse skin ($n = 3$, $*p < 0.05$ vs Gel). k) Average adhesion work of HA-PG bulk gels and patches on mouse skin ($n = 3$, $**p < 0.01$ vs Gel).

in mechanical and degradation properties might be attributed to much denser fibrillary internal structure of HA-PG patch compared to HA-PG bulk gel, as observed in SEM analysis (Figure 6g). XPS analysis of HA-PG patch and bulk gel indicated that surface exposure of functional groups and chemical moieties (e.g., oxidized catechols, quinone) for cross-linking and interaction with nucleophiles was increased on the HA-PG patch compared with HA-PG bulk gel (Figure S9, Supporting Information), due to highly dense nanofibrillar internal structures in the patch. Therefore, the HA-PG patch exhibited significantly improved tissue adhesion compared to the HA-PG bulk gel. The tissue adhesiveness of the HA-PG patch and gel was compared with the samples cross-linked *in vivo* by auto-oxidation after administration into subcutaneous pocket of mouse. Rheometric analysis in a tack test mode of the HA-PG samples

adhered to skin tissues (Figure 6h) indicated that the adhesion force of the patch (3.9 ± 0.5 N) to skin tissue was more than twofold greater than that of the bulk gel (1.4 ± 0.3 N) (Figure 6i, j) and the work required to detach HA-PG construct from skin tissue was much larger in the case of patch (2.6 ± 0.3 mJ) than the bulk gel (1.0 ± 0.3 mJ) (Figure 6k). Together, these results demonstrate that the change from bulk gel to patch improved physical, mechanical, and adhesive properties of HA-PG hydrogel, which is similar to HA-CA hydrogel.

2.9. Oxidant-Free HA-PG Patch for Biomedical Applications

Finally, the off-the-shelf availability of oxidant-free HA-PG hydrogel patch was tested for cell transplantation and drug

delivery. The HA-PG patch did not show cytotoxicity when it was applied for hADSC culture (Figure S10, Supporting Information). HA-PG patch could readily form 3D hydrogel on the tissues via auto-oxidation reaction by in vivo oxidative condition even without the use of an oxidant agent (NaIO_4) for cross-linking. Using its great tissue adhesiveness and ability to in vivo auto-oxidation, HA-PG patch was able to efficiently deliver stem cell-derived organoids to wet tissues in a noninvasive manner through simple two-step processes; organoid loading and taping with HA-PG patch without oxidant cross-linker (Figure 7a). The successful engraftment of DiI-labeled intestinal and liver organoids using oxidant-free HA-PG patch was visualized onto the surface of the small intestine and liver lobe, respectively (Figure 7b,c). Thus, our HA-PG hydrogel patch platform can improve the regenerative potential of organoid technology for cell therapy and tissue engineering. In addition to massive organoids, single cell type of DiI-labeled hADSCs were also efficiently transplanted to various wet tissues including intestine, liver, kidney, and stomach by attaching the patch onto tissue surface and then seeding cells on the patch in an oxidant-free manner (Figure S11, Supporting Information). These results indicate that the HA-PG hydrogel patch can provide a versatile biomaterial platform for cell therapy regardless of target organs or cell types like HA-CA hydrogel patch.

As another biomedical application, the HA-PG patch-based drug delivery system was tested for diabetic wound healing. Platelet-derived growth factor (PDGF), one of the growth factors that play an important role in all phases of wound healing,^[34] was loaded to HA-PG patch and bulk gel for topical delivery. Due to strong binding of PDGF to gallol moiety of HA-PG, PDGF was hardly released from both HA-PG patch and bulk gel in the absence of hyaluronidase under physiological condition (in PBS at 37 °C) (Figure 7d). In the presence of hyaluronidase (20 U per sample), PDGF was sustainably released from the patches for 5 d as HA network gradually degraded, while burst release of PDGF from bulk gel was observed within 6 h likely due to rapid degradation of HA network (Figures 6d and 7d). This result suggests that HA-PG patch-mediated drug delivery would be more efficient than bulk gel-mediated drug delivery for therapeutic approaches. To evaluate therapeutic efficacy of the PDGF-loaded HA-PG patch in a full-thickness skin wound model of streptozotocin-induced diabetic mouse with impaired healing capacity owing to constant tissue damage and chronic inflammation,^[35] the HA-PG patch containing PDGF was topically applied by attaching drug-loaded patch onto the wounded region of skin without oxidant treatment (Figure 7e). The application of PDGF-loaded HA-PG patches (patch loaded with PDGF in situ after

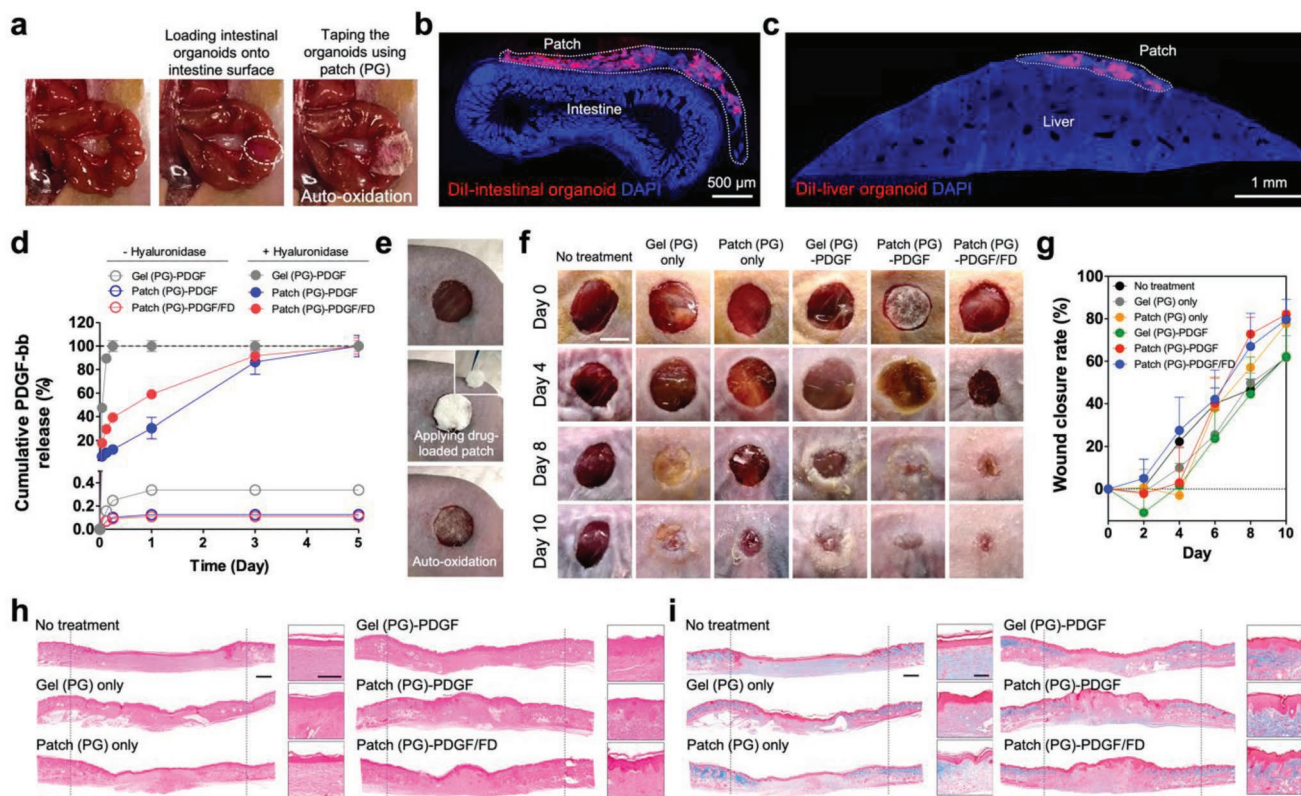


Figure 7. Biomedical applications of oxidant-free HA-PG patches. a) Procedures for HA-PG patch-mediated transplantation of intestinal organoids onto the mouse intestine. Fluorescence images to confirm the engraftment of b) DiI-labeled intestinal organoids onto the mouse intestine (scale bar = 500 μm) and c) DiI-labeled liver organoids onto the mouse liver lobe one day after transplantation (scale bar = 1 mm). d) Comparison of PDGF release profiles of HA-PG patch and bulk solution hydrogel with or without hyaluronidase treatment ($n = 4$). e) Procedures for drug delivery using HA-PG patch on skin wound in an oxidant-free manner. f) Representative photos of skin wound closure in diabetic mice at day 0, 4, 8, and 10. Scale bar = 5 mm. g) The wound closure rate in diabetic mice up to day 10 after treatments ($n = 5-7$). h) H&E-stained images of the treated diabetic skin wounds at day 10. Scale bars = 500 μm (left column) and 200 μm (right column). i) Collagen deposition in the treated diabetic skin wounds at day 10, as confirmed by Masson's trichrome staining. Scale bars = 500 μm (left column) and 200 μm (right column).

attaching the patch onto the wound site; Patch-PDGF group and patch preloaded with PDGF before lyophilization; Patch-PDGF/FD group) accelerated wound healing compared to other control groups including HA-PG bulk gel loaded with PDGF (Gel-PDGF group) (Figure 7f,g). H&E and MT staining revealed later stages of wound healing process containing regenerated hair follicles and extensive collagen deposition in Patch-PDGF and Patch-PDGF/FD groups (Figure 7h,i). Like the HA-CA patch experiments for VEGF delivery, we confirmed the equivalency of patches preloaded with PDGF to patches with in situ PDGF loading in terms of therapeutic efficacy for wound healing (Figure 7f–i). Together, these results from diabetic wound model support that oxidant-free HA-PG patches with preloaded growth factors could be developed as an off-the-shelf drug delivery product for therapeutic applications, providing a great convenience for medical institutes and hospitals.

2.10. Verification of the Stability and Biosafety of Phenolic HA Patches

We verified the long-term stability of phenolic HA materials because catechol- and gallol-modified materials are prone to be oxidized during synthesis and storage due to the presence of phenolic hydroxyl groups. To verify the stability of HA-CA and HA-PG conjugates, chemical analysis using Fourier transform infrared (FT-IR) spectroscopy was performed with different batches of the conjugates (new batch: the samples right after synthesis, old batch: the samples synthesized one year ago), and the FT-IR spectrum of those batches was compared with that of the oxidized samples by oxidizing reagent. HA-CA synthesized one year ago (old batch) and newly synthesized HA-CA (new batch) exhibited similar FT-IR spectra each other in the whole wavelength ranges (Figure S12a, Supporting Information), indicating that there was no change in chemical structure of HA-CA over a long period of storage. On the other hand, the FT-IR spectrum of fully oxidized HA-CA samples by oxidant (NaIO_4) treatment was quite different from those of non-oxidized HA-CA conjugate samples from new and old batches (Figure S12a, Supporting Information). The peak at 792 cm^{-1} , indicating the formation of biphenols,^[36] was detected only in the oxidized HA-CA sample and the peak related to the C–C stretching vibration of the aromatic ring in the oxidized HA-CA slightly shifted from 1410 (old batch)/ 1416 cm^{-1} (new batch) to 1384 cm^{-1} , which demonstrated the deformation of the aromatic ring induced by oxidation of catechol groups of HA-CA conjugate.^[37] Likewise, FT-IR spectra of HA-PG samples showed the same trends as HA-CA samples. There was no significant difference between the FT-IR spectra of HA-PG conjugates right after synthesis (new batch) and synthesized one year ago (old batch) (Figure S12b, Supporting Information). In contrast, new peak appearance at 790 cm^{-1} and peak shift from $1416/1417$ to 1412 cm^{-1} were observed in the oxidant-treated HA-PG sample, indicating changes in chemical structure triggered by oxidation of gallol groups. Actually, both new and old batches of HA-CA/PDGF conjugates formed hydrogels upon exposure to oxidant (NaIO_4) (Figure S12c,d, Supporting Information). All together, these results demonstrate that our synthesis protocol can generate HA-CA/PDGF conjugates with marginal oxidation and the

conjugates are highly stable without any changes in chemical structure during long-term storage.

In addition, we further verified the biosafety of our phenolic HA patches in vitro and in vivo. We previously demonstrated that various primary cells and stem cells including hepatocytes, endothelial cells, neural stem cells, and mesenchymal stem cells were highly viable in HA-CA hydrogels during culture.^[7a,8,38] We also reported that hADSCs grown within gallol-modified HA hydrogel showed good viability more than 95%.^[7b] In the current study, the viability of organoids derived from different organs (liver, intestine, and stomach) was examined using Live/Dead staining assay. There were few dead cells in all types of organoids encapsulated within HA-CA/PDGF patches (Figure S13a,b, Supporting Information), indicating excellent biocompatibility of the phenolic HA patches again. The degradation products from HA-CA/PDGF hydrogels (e.g., catechol/gallol fragments, benzoquinone) may cause potential toxicity in vivo. However, HA hydrogels usually undergo enzymatic degradation of HA backbone in vivo, and thus the degradation products from HA-CA/PDGF hydrogels seem to mostly exist as forms of molecules bound to cleaved HA fragments rather than as single molecules. Therefore, such adjunct forms of degradation products may show much less toxicity than single molecules of oxidized catechol, gallol, and quinone. To verify the biosafety of our hydrogel patches in vivo, we implanted HA-CA/PDGF patches into mouse subcutaneous space and conducted histological analyses with skin tissues adjacent to hydrogel patches harvested at 1 and 2 weeks after implantation. H&E and toluidine blue staining revealed that both HA-CA and HA-PG patches did not induce any detectable inflammatory responses and tissue necrosis in surrounding tissues at all experimental time points (Figure S14a,b, Supporting Information). Actually, several previous studies including ours have also reported marginal toxicity of catechol- or gallol-modified hydrogels in vivo when they were applied to various tissues and organs including liver, heart, kidney, and skin.^[7,39] More recently, Shin et al. evaluated toxicity of materials modified with tannic acid, a highly branched polyphenol with five gallol groups and five catechol groups, over 29 d by injecting them to rats biweekly, and observed that there was no evidence of significant toxicity for the whole period of test.^[40] Together, we speculate that our HA-CA/PDGF hydrogel patches may provide safe biomaterials for cell therapy and drug delivery though long-term toxicity, carcinogenic potential, and adverse effects such as chronic inflammation and foreign body reaction need to be further monitored.

3. Conclusions

Here, we demonstrate a novel concept to utilize tissue-adhesive HA hydrogel patches capable of working as tissue tape which are easy to fabricate and handle, allowing for highly reliable, noninvasive stem cell therapy and drug delivery. Bioinspired HA-CA/PDGF hydrogel patches were prepared into lyophilized hydrogels, which are ready-to-use for cell transplantation and drug delivery irrespective of cell type or target tissue, providing off-the-shelf availability. The HA-CA/PDGF hydrogel patches exhibit much stronger tissue adhesiveness and greater elastic modulus than the bulk solution gel form and, accordingly, can

be easily applied for effective cell delivery onto several target organs, including dynamically beating hearts, without any invasive or complicated procedures. Large cell clusters, which are difficult to transplant with conventional injection methods and delivery materials, such as organoids, can also be easily administered into target organs using these patches. The HA-CA/PG patches also showed excellent performance as a drug-loaded tissue tape ready-made for topical drug delivery to promote wound healing. Based on the proof-of-concept described here, further preclinical studies using large animal models, including pigs and nonhuman primates, are required for successful translation of our approach to clinics. Although further improvement is needed for its clinical translation, our HA hydrogel patch platforms offer a novel, innovative, and versatile strategy for stem cell therapy, drug delivery, and tissue engineering. Considering recent highlights on development of functional hydrogels for translational biomedicine,^[41] the application of our HA hydrogel patches could be extended to a wide variety of translational biomedicine such as sensors, actuators, and bioelectronics.

Supporting Information

Supporting Information is available from the Wiley Online Library or from the author.

Acknowledgements

This research was supported by grants (2017R1A2B3005994 and 2018M3A9H1021382) of the National Research Foundation of Korea (NRF) funded by the Korean government, the Ministry of Science, and ICT (MSIT). This research was also supported by the Institute for Basic Science (IBS-R026-D1). The authors thank Dr. Hyo Jin Kang (Department of Plastic and Reconstructive Surgery, Seoul National University Bundang Hospital) for technical support on the rat myocardial infarction study. SD rats (Orient Bio Inc., Seongnam, Korea) were cared for according to the Association for Assessment and Accreditation of Laboratory Animal Care International System. All animal experiments were performed according to the International Guide for the Care and Use of Laboratory Animals. Experimental procedures were monitored and approved by the Animal Research Committee of Yonsei University College of Medicine (IACUC No. 2012-0202-2).

Conflict of Interest

The authors declare no conflict of interest.

Keywords

drug delivery, hyaluronic acid, off-the-shelf availability, phenolic adhesive hydrogel patch, stem cell therapy

Received: May 14, 2019

Revised: August 1, 2019

Published online: September 2, 2019

- [1] a) D. R. Griffin, W. M. Weaver, P. O. Scumpia, D. Di Carlo, T. Segura, *Nat. Mater.* **2015**, *14*, 737; b) S. B. Seif-Naraghi, J. M. Singelyn, M. A. Salvatore, K. G. Osborn, J. J. Wang, U. Sampat, O. L. Kwan, G. M. Strachan, J. Wong, P. J. Schup-Magoffin, *Sci. Transl. Med.* **2013**, *5*, 173ra25.

- [2] a) J. J. Green, J. H. Elisseeff, *Nature* **2016**, *540*, 386; b) B. G. Ballios, M. J. Cooke, D. van der Kooy, M. S. Shoichet, *Biomaterials* **2010**, *31*, 2555.
- [3] a) J. Li, D. J. Mooney, *Nat. Rev. Mater.* **2016**, *1*, 16071; b) S. Zhang, J. Ermann, M. D. Succi, A. Zhou, M. J. Hamilton, B. Cao, J. R. Korzenik, J. N. Glickman, P. K. Vemula, L. H. Glimcher, *Sci. Transl. Med.* **2015**, *7*, 300ra128.
- [4] M. H. Chen, L. L. Wang, J. J. Chung, Y.-H. Kim, P. Atluri, J. A. Burdick, *ACS Biomater. Sci. Eng.* **2017**, *3*, 3146.
- [5] a) S. T. Wall, J. C. Walker, K. E. Healy, M. B. Ratcliffe, J. M. Guccione, *Circulation* **2006**, *114*, 2627; b) H. Wang, C. B. Rodell, M. E. Lee, N. N. Dusaj, J. H. Gorman III, J. A. Burdick, R. C. Gorman, J. F. Wenk, *J. Biomech.* **2017**, *7*, 31.
- [6] A. S. Hoffman, *Adv. Drug Delivery Rev.* **2012**, *64*, 18.
- [7] a) J. Shin, J. S. Lee, C. Lee, H. J. Park, K. Yang, Y. Jin, J. H. Ryu, K. S. Hong, S. H. Moon, H. M. Chung, *Adv. Funct. Mater.* **2015**, *25*, 3814; b) J. H. Cho, J. S. Lee, J. Shin, E. J. Jeon, S. An, Y. S. Choi, S. W. Cho, *Adv. Funct. Mater.* **2018**, *28*, 1705244.
- [8] a) S. Hong, K. Yang, B. Kang, C. Lee, I. T. Song, E. Byun, K. I. Park, S. W. Cho, H. Lee, *Adv. Funct. Mater.* **2013**, *23*, 1774; b) H.-J. Park, Y. Jin, J. Shin, K. Yang, C. Lee, H. S. Yang, S.-W. Cho, *Biomacromolecules* **2016**, *17*, 1939.
- [9] K. L. Fujimoto, K. Tobita, W. D. Merryman, J. Guan, N. Momoi, D. B. Stolz, M. S. Sacks, B. B. Keller, W. R. Wagner, *J. Am. Coll. Cardiol.* **2007**, *49*, 2292.
- [10] R. Battino, H. L. Clever, *Chem. Rev.* **1966**, *66*, 395.
- [11] a) H. Lee, J. Rho, P. B. Messersmith, *Adv. Mater.* **2009**, *21*, 431; b) K. Yang, J. S. Lee, J. Kim, Y. B. Lee, H. Shin, S. H. Um, J. B. Kim, K. I. Park, H. Lee, S.-W. Cho, *Biomaterials* **2012**, *33*, 6952.
- [12] K. Li, S. Cai, *Soft Matter* **2014**, *10*, 8202.
- [13] a) I. M. Barbash, P. Chouraqui, J. Baron, M. S. Feinberg, S. Etzioni, A. Tessone, L. Miller, E. Guetta, D. Zipori, L. H. Kedes, *Circulation* **2003**, *108*, 863; b) Y. Miyahara, N. Nagaya, M. Kataoka, B. Yanagawa, K. Tanaka, H. Hao, K. Ishino, H. Ishida, T. Shimizu, K. Kangawa, *Nat. Med.* **2006**, *12*, 459.
- [14] S. H. Kim, H.-H. Moon, H. A. Kim, K.-C. Hwang, M. Lee, D. Choi, *Mol. Ther.* **2011**, *19*, 741.
- [15] M. G. S. J. Sutton, N. Sharpe, *Circulation* **2000**, *101*, 2981.
- [16] a) T. Kinnaird, E. Stabile, M. Burnett, C. Lee, S. Barr, S. Fuchs, S. Epstein, *Circ. Res.* **2004**, *94*, 678; b) M. F. Pittenger, B. J. Martin, *Circ. Res.* **2004**, *95*, 9; c) A. I. Caplan, D. Correa, *Cell Stem Cell* **2011**, *9*, 11.
- [17] W.-H. Zimmermann, I. Melnychenko, G. Wasmeier, M. Didié, H. Naito, U. Nixdorff, A. Hess, L. Budinsky, K. Brune, B. Michaelis, *Nat. Med.* **2006**, *12*, 452.
- [18] a) D. Kai, Q.-L. Wang, H.-J. Wang, M. P. Prabhakaran, Y. Zhang, Y.-Z. Tan, S. Ramakrishna, *Acta Biomater.* **2014**, *10*, 2727; b) D.-H. Kim, R. R. Smith, P. Kim, E. H. Ahn, H.-N. Kim, E. Marbán, K.-Y. Suh, A. Levchenko, *Integr. Biol.* **2012**, *4*, 1019.
- [19] A. Duarte, J. Coelho, J. Bordado, M. Cidade, M. Gil, *Prog. Polym. Sci.* **2012**, *37*, 1031.
- [20] a) S. Jiang, P. Li, Y. Yu, J. Liu, Z. Yang, *J. Biomech.* **2014**, *47*, 3344; b) S. Badaan, D. Petrisor, C. Kim, P. Mozer, D. Mazilu, L. Gruionu, A. Patriciu, K. Cleary, D. Stoianovici, *Int. J. Med. Rob. Comput. Assisted Surg.* **2011**, *7*, 138.
- [21] M. Domenech, L. Polo-Corrales, J. E. Ramirez-Vick, D. O. Freytes, *Tissue Eng., Part B* **2016**, *22*, 438.
- [22] a) M. Kawamura, S. Miyagawa, K. Miki, A. Saito, S. Fukushima, T. Higuchi, T. Kawamura, T. Kuratani, T. Daimon, T. Shimizu, T. Okano, Y. Sawa, *Circulation* **2012**, *126*, S29; b) H. Masumoto, T. Matsuo, K. Yamamizu, H. Uosaki, G. Narazaki, S. Katayama, A. Marui, T. Shimizu, T. Ikeda, T. Okano, *Stem Cells* **2012**, *30*, 1196.
- [23] H.-J. Wei, C.-H. Chen, W.-Y. Lee, I. Chiu, S.-M. Hwang, W.-W. Lin, C.-C. Huang, Y.-C. Yeh, Y. Chang, H.-W. Sung, *Biomaterials* **2008**, *29*, 3547.

- [24] J. Ge, L. Guo, S. Wang, Y. Zhang, T. Cai, R. C. Zhao, Y. Wu, *Stem Cell Rev. Rep.* **2014**, *10*, 295.
- [25] S. Kim, A. N. Cho, S. Min, S. Kim, S. W. Cho, *Adv. Ther.* **2019**, *2*, 1800087.
- [26] S. Yui, T. Nakamura, T. Sato, Y. Nemoto, T. Mizutani, X. Zheng, S. Ichinose, T. Nagaishi, R. Okamoto, K. Tsuchiya, *Nat. Med.* **2012**, *18*, 618.
- [27] K. P. O'Rourke, E. Loizou, G. Livshits, E. M. Schatoff, T. Baslan, E. Manchado, J. Simon, P. B. Romesser, B. Leach, T. Han, *Nat. Biotechnol.* **2017**, *35*, 577.
- [28] a) T. Takebe, K. Sekine, M. Enomura, H. Koike, M. Kimura, T. Ogaeri, R.-R. Zhang, Y. Ueno, Y.-W. Zheng, N. Koike, *Nature* **2013**, *499*, 481; b) R.-R. Zhang, M. Koido, T. Tadokoro, R. Ouchi, T. Matsuno, Y. Ueno, K. Sekine, T. Takebe, H. Taniguchi, *Stem Cell Rep.* **2018**, *10*, 780.
- [29] a) M. Huch, H. Gehart, R. van Boxtel, K. Hamer, F. Blokzijl, M. M. Verstegen, E. Ellis, M. van Wenum, S. A. Fuchs, J. de Ligt, *Cell* **2015**, *160*, 299; b) M. Huch, C. Dorrell, S. F. Boj, J. H. van Es, V. S. Li, M. van De Wetering, T. Sato, K. Hamer, N. Sasaki, M. J. Finegold, *Nature* **2013**, *494*, 247.
- [30] A. Higuchi, Q.-D. Ling, Y.-A. Ko, Y. Chang, A. Umezawa, *Chem. Rev.* **2011**, *111*, 3021.
- [31] E. J. Rebar, Y. Huang, R. Hickey, A. K. Nath, D. Meoli, S. Nath, B. Chen, L. Xu, Y. Liang, A. C. Jamieson, *Nat. Med.* **2002**, *8*, 1427.
- [32] C. Lee, J. Shin, J. S. Lee, E. Byun, J. H. Ryu, S. H. Um, D.-I. Kim, H. Lee, S.-W. Cho, *Biomacromolecules* **2013**, *14*, 2004.
- [33] a) D. C. West, D. M. Shaw, P. Lorenz, N. S. Adzick, M. T. Longaker, *Int. J. Biochem. Cell Biol.* **1997**, *29*, 201; b) M. Fronza, G. F. Caetano, M. N. Leite, C. S. Bitencourt, F. W. Paula-Silva, T. A. Andrade, M. A. Frade, I. Merfort, L. H. Faccioli, *PLoS One* **2014**, *9*, e112297.
- [34] J. Ishihara, A. Ishihara, K. Fukunaga, K. Sasaki, M. J. White, P. S. Briquez, J. A. Hubbell, *Nat. Commun.* **2018**, *9*, 2163.
- [35] V. Falanga, *Lancet* **2005**, *366*, 1736.
- [36] P. J. Linstrom, W. G. Mallard, *NIST Chemistry WebBook, NIST Standard Reference Database Number 69*, National Institute of Standards and Technology, Gaithersburg, MD **2011**, <http://webbook.nist.gov>.
- [37] V. A. Minaeva, B. F. Minaev, G. V. Baryshnikov, O. M. Romeyko, M. Pittelkow, *Vib. Spectrosc.* **2013**, *65*, 147.
- [38] B. Kang, J. Shin, H.-J. Park, C. Rhyou, D. Kang, S.-J. Lee, Y.-s. Yoon, S.-W. Cho, H. Lee, *Nat. Commun.* **2018**, *9*, 5402.
- [39] a) E. Park, J. Lee, K. M. Huh, S. H. Lee, H. Lee, *Adv. Healthcare Mater.* **2019**, *8*, 1900275; b) L. Han, L. Yan, K. Wang, L. Fang, H. Zhang, Y. Tang, Y. Ding, L.-T. Weng, J. Xu, J. Weng, *NPG Asia Mater.* **2017**, *9*, e372.
- [40] M. Shin, H.-A. Lee, M. Lee, Y. Shin, J.-J. Song, S.-W. Kang, D.-H. Nam, E. J. Jeon, M. Cho, M. Do, *Nat. Biomed. Eng.* **2018**, *2*, 304.
- [41] a) K. Xue, X. Wang, P. W. Yong, D. J. Young, Y. L. Wu, Z. Li, X. J. Loh, *Adv. Ther.* **2019**, *2*, 1800088; b) Z. X. Zhang, D. J. Young, Z. Li, X. J. Loh, *Small Methods* **2019**, *3*, 1800270; c) Z. W. K. Low, Z. Li, C. Owh, P. L. Chee, E. Ye, D. Kai, D. P. Yang, X. J. Loh, *Small* **2019**, *15*, 1805453; d) K. Xue, S. S. Liow, A. A. Karim, Z. Li, X. J. Loh, *Chem. Rec.* **2018**, *18*, 1517.